Antibacterial properties of photo-crosslinked chitosan/ methacrylated hyaluronic acid nanoparticles loaded with bacitracin

Raquel R. Gonçalves, Daniela Peixoto, Rui R. Costa, Albina R. Franco, Vânia I.B. Castro, Ricardo A. Pires, Rui L. Reis, Iva Pashkuleva, Devid Maniglio, Annalisa Tirella, Antonella Motta, Natália M. Alves

PII: S0141-8130(24)05055-4

DOI: https://doi.org/10.1016/j.ijbiomac.2024.134250

Reference: BIOMAC 134250

To appear in: *International Journal of Biological Macromolecules*

Received date: 15 March 2024

Revised date: 25 July 2024

Accepted date: 27 July 2024

Please cite this article as: R.R. Gonçalves, D. Peixoto, R.R. Costa, et al., Antibacterial properties of photo-crosslinked chitosan/methacrylated hyaluronic acid nanoparticles loaded with bacitracin, *International Journal of Biological Macromolecules* (2024), https://doi.org/10.1016/j.ijbiomac.2024.134250

Antibacterial properties of photo-crosslinked chitosan/methacrylated hyaluronic acid nanoparticles loaded with bacitracin

Raquel R. Gonçalves[a,b,c], Daniela Peixoto[a,b], Rui R. Costa[a,b], Albina R. Franco[a,b], Vânia I.B. Castro[a,b], Ricardo A. Pires[a,b], Rui L. Reis[a,b], Iva Pashkuleva[a,b], Devid Maniglio[c], Annalisa Tirella[c], Antonella Motta[c], Natália M. Alves[a,b,*]

[a] *3B's Research Group, I3Bs – Research Institute on Biomaterials, Biodegradables and Biomimetics, University of Minho, Headquarters of the European Institute of Excellence on Tissue Engineering and Regenerative Medicine, AvePark, Parque de Ciência e Tecnologia, Zona Industrial da Gandra, 4805-017 Barco, Guimarães, Portugal*

[b] *ICVS/3B's–PT Government Associate Laboratory, Braga/Guimarães, Portugal*

[c] *BIOtech Research Center, Department of Industrial Engineering, University of Trento, Via Delle Regole 101, 38123 Trento, Italy*

*Corresponding author.

E-mail addresses: nalves@i3bs.uminho.pt

TOTAL NUMBER OF WORDS: 7565 words

NUMBER OF TABLES: 2 tables

NUMBER OF FIGURES: 8 figures

ABSTRACT

The current treatments for wounds often fail to produce adequate healing, leaving wounds vulnerable to persistent infections and development of drug-resistant microbial biofilms. New natural-derived nanoparticles were studied to impair bacteria colonization and hinder the formation of biofilms in wounds. The nanoparticles were fabricated through polyelectrolyte complexation of chitosan (CS, polycation) and hyaluronic acid (HA, polyanion). UV-induced photo-crosslinking was used to enhance the stability of the nanoparticles. To achieve this, HA was methacrylated (HAMA, degree of modification of 20 %). Photo-crosslinked nanoparticles obtained from HAMA and CS had a diameter of 478 nm and a more homogeneous size distribution than nanoparticles assembled solely through complexation (742 nm). The nanoparticles were loaded with the antimicrobial agent bacitracin (BC), resulting in nanoparticles with a diameter of 332 nm. The encapsulation of BC was highly efficient (97 %). The BC-loaded nanoparticles showed significant antibacterial activity against gram-positive

bacteria *Staphylococcus aureus*, *Methicillin-resistant S. aureus* and *S. epidermidis*. The nanoparticles loaded with BC based on photo-crosslinked HAMA/CS demonstrated inhibition of biofilm formation and a positive effect on the proliferation of mammalian cells (L929). These crosslinked nanoparticles have potential for the long-term treatment of wounds and controlled antibiotic delivery at the location of a lesion.

Keywords: Nanoparticles, Methacrylated Hyaluronic Acid, Photo-crosslinking, Bacitracin, Chronic Wounds

1. Introduction

Wound healing is the natural physiological response that occurs when a tissue recovers from damage, a process that involves hemostasis, inflammation, proliferation, and remodeling [1,2]. Some wounds are characterized by a full-thickness depth, excessive inflammatory response, and slow healing, becoming chronic wounds or ulcers. When wounds do not heal in a timely manner, they often develop persistent infections and form drug-resistant microbial biofilms [3]. Their development is linked to underlying conditions such as ischemia, diabetes, venous stasis disease, obesity, and age [4,5]. Current wound healing treatments used in clinics are based on prevention and early detection. After diagnosis, the adopted measures include cleansing and debridement, infection and inflammation control, pressure redistribution, restoration of tissue perfusion measures, and advanced cell therapies. These approaches can be used alone or can be combined to boost the healing process [6–8]. Nonetheless, these approaches frequently fail to completely close ulcers, which can only be solved by amputations and result in a lower quality of life for patients, and in some cases, even death[9,10]. Such poor clinical outcomes demonstrate that new wound healing treatments and devices are needed.

Nanomaterials have demonstrated to be a promising tool to enhance wound healing. Numerous studies have shown that nanoparticles improve stability, cross-membrane transport, circulation time, safety, and are efficient in encapsulating drugs, such as antibiotics [11–13]. Nanoparticulate systems can be readily produced from charged biomacromolecules via electrostatic interactions. For example, chitosan (CS) and hyaluronic acid (HA) are common polyelectrolytes used to generate nanocomplexes [14]. CS is a linear polycation widely used in drug delivery and in wound dressings [15,16] due to its antibacterial properties [17] and ability to modulate inflammatory

processes [18]. HA is a linear polyanionic glycosaminoglycan involved in the homeostasis of tissue hydration and the remodeling of the extracellular matrix (ECM) following injury [19,20]. Previous studies have shown that CS and HA generate feasible and versatile systems for an efficient delivery of bioactive substances. For example, Parajó *et al*. demonstrated the efficiency of CS/HA nanoparticles in delivering pro-angiogenic growth factor s[21], whereas Tirella *et al*. showed the ability for siRNA delivery [22]. Similarly, Lallana *et al*. showed that larger negatively charged RNA can be loaded into CS/HA nanoparticles[23]. Yang *et al*. further showcased that CS/HA nanoparticles can also serve as nanovehicles for water-insoluble substances such as curcuminoid [24]. In the study by Lima *et al.*, functionalized CS/HA nanoparticles demonstrated successful internalization under normal and pro-inflammatory states in primary human articular chondrocytes, as well as in human umbilical vein endothelial cells, and human monocytes [25].

Because of their physicochemical characteristics, nanoscale size, and ease of the complexation reaction, CS and HA offer specific benefits in wound treatment. Nonetheless, these biomaterials can be chemically modified with functional groups to enhance the potential of ionically crosslinked constructs for wound healing, such as increasing the crosslinking density and colloidal stability [26,27]. In this study, we used polyelectrolyte complexation to produce nanoparticles based on CS and a methacrylate-modified HA to make it UV photo-crosslinkable. Photo-crosslinking has been shown to be a method for tuning mechanical properties and drug loading capacity of hydrogels while maintaining biocompatibility [28,29]. Although photo-crosslinking has been seldom applied to particulate systems, it has improved the loading and delivery of gene-based therapeutics from acrylate-derived nanoparticle matrices [26,30].

The effect of the photo-crosslinking post-treatment on the size, uniformity, and stability of the complex nanoparticles was evaluated [31]. The ability of the developed nanoparticles to serve as drug vehicles is demonstrated by the encapsulation of bacitracin, a cyclic polypeptide antibiotic effective against gram-positive bacteria used for the short-term prevention and treatment of infections [32]. The antibacterial efficacy of BC-loaded NPs against bacteria responsible for wound infections was showcased, indicating that the developed nanoparticles have the potential to treat acute and chronic skin infections.

2. Materials and methods

2.1. Materials

Dried Sodium Hyaluronate (HA) (molecular weight: 151 - 300 kDa) was purchased from LifeCore. Chitosan (CS) (low molecular weight: 50-190 kDa, ≥75.0 % deacetylation), bacitracin zinc salt (from Bacillus licheniformis, ~70,000 U/g), methacrylic anhydride (MA, topanol A 2.000 ppm inhibitor, 94 %), lithium phenyl-2,4,6-trimethylbenzoylphosphinate photoinitiator (LAP, purity ≥95 %), and PBS tablets were purchased from Sigma-Aldrich. Membranes Spectra/Por 3, cut-off 3.5 kDa were purchased from Fisher Scientific. Hydrochloric acid (HCl) was purchased from Honeywell. Sodium hydroxide (NaOH) was purchased from Panreac. Mueller-Hinton (MH) agar and Tryptic Soy (TS) Broth were purchased from Neo Biotech.

2.2. Synthesis of Methacrylated Hyaluronic Acid

Methacrylated HA (HAMA) was synthesized using an adapted protocol from Loebe *et al*. [33]. Briefly, a solution of 6 mg/mL HA was prepared in ultra-pure water and left stirring overnight. The solution was placed in an ice bath and the pH was adjusted to 8.5 by dropwise addition of 1M NaOH under stirring. The methacrylation was performed by the slow addition of methacrylic anhydride to the HA solution (1.5 mL per gram of HA) at pH 8.5 (pH continuously adjusted with 5 M NaOH). The reaction was carried overnight at room temperature and finally, the pH was readjusted to 8.5. Unreacted chemicals were removed by dialysis (membranes Spectra/Por 3, cut-off 3.5 kDa) against osmotized water (OW). The final product was lyophilized and stored at -20 °C. The success of the modification was confirmed by ^{1}H NMR (Bruker Avance, 400 MHz) and the spectra were integrated to calculate the degree of the substitution.

2.3. Preparation of Nanoparticles Based on Chitosan and Hyaluronic Acid

Nanoparticles were produced following a protocol adapted from Tirella *et al.* [22] and Lallana *et al*. [34]. Briefly, a CS solution was prepared at a concentration of 0.69 mg/mL in HCl (4.6 mM). HA (1.67 mg/mL), HAMA (1.67 mg/mL), and LAP (3.75 mg/mL) solutions were prepared in OW (pH = 5). All solutions were stirred

gently overnight followed by an adjustment of the pH to 5 using NaOH (0.1 M) and HCl (0.1 M). CS (250 μL) was diluted in an equal volume of OW (20 min at 1000 rpm). The resulting 500 μL solution was gently poured into an equal volume of HA or HAMA to obtain HA/CS or HAMA/CS with a mass ratio of 31/100. To obtain photo-crosslinked nanoparticles, LAP was also added to the HAMA solution at a HAMA:LAP volume ratio of 9:1, to initiate the photopolymerization. The mixture was stirred for 30 min at room temperature. The cross-linking of HAMA/CS nanoparticles was made by UV irradiation with a UV lamp (Model Triwood 6/36, λ = 352 nm, P = 6 W) for 1 min. Three different formulations were prepared: HA/CS, HAMA/CS and crosslinked HAMA/CS (HAMA/CS-Xlinked).

2.4. Characterization of Nanoparticles

The hydrodynamic diameter and zeta potential of the obtained nanoparticles were determined by dynamic light scattering (DLS) using a Malvern Nano-ZS zeta-sizer and the Zetasizer Nano v7.19 software. Aliquots with 1 mL were loaded in polystyrene disposable cuvettes and size distribution, z-average and polydispersity index (PDI) were determined. The samples were prepared to ensure a count rate between 250–400 kcps. Zeta potential measurements were performed using folded capillary cells. All measurements were made in triplicates.

The morphology of the nanoparticles was analyzed by scanning electron microscopy (SEM, JSM-6010 LV, JEOL). Sample preparation was performed by centrifuging a nanoparticle suspension at 10000 rpm, discarding the supernatant, and lyophilization. The dry nanoparticles were immobilized on carbon tape and sputtered with platinum.

2.5. Nanoparticle Stability

The nanoparticles were suspended in 1 mL of OW at 25 and 37 °C for 0, 3, 7 and 14 days. After these periods, the size distribution, z-average, and PDI were measured as above described. The data is presented as the averaged results of three independent experiments.

2.6. Encapsulation of Bacitracin in Crosslinked Nanoparticles (BC-loaded HAMA/CS-Xlinked nanoparticles

BC was loaded on HAMA/CS-Xlinked nanoparticles, adapted from the protocols of Tirella *et al.* [22] and Lallana *et al*. [34]. First, BC was dissolved in OW at a concentration of 0.42 mg/mL (Fig. S3) [35]. This solution was added to an equal volume of CS at 0.69 mg/mL and they were mixed for 20 min at 1000 rpm. 500 µL of the resulting mixture was poured into an equal volume of the HAMA/LAP solution (as described in Section 2.3). After 30 min, the NPs were irradiated with a UV lamp (Model Triwood 6/36, λ = 352 nm) for 1 min. The loaded nanoparticles were characterized by DLS and SEM. The BC encapsulation efficiency was determined by analytical High-Performance Liquid Chromatography (HPLC, Alliance, Waters Corporation, USA) using a C18 Atlantis column (250 mm x 4.6 mm, 5 µm, Waters Corporation, USA). The samples were passed through a 0.22 µm pore size filter and 10 µL was injected. The isocratic method was applied using Phosphate buffer 0.5 M and methanol (30:70) at a flow rate of 1 mL/min [36]. The detection wavelength was performed at 254 nm and the elution time was 30 min.

2.7. Antibacterial Activity of BC-loaded HAMA/CS-Xlinked nanoparticles

2.7.1 Radial diffusion assay

The antibacterial activity of BC-loaded HAMA/CS-Xlinked nanoparticles was evaluated against different well-known wound infecting Gram-positive pathogens [37], namely *Staphylococcus aureus* ATCC 2592*3 (S. aureus)*, Methicillin-resistant *S. aureus* ATCC 700698 (MRSA) and *Staphylococcus epidermidis* ATCC 12228 *(S. epidermidis).* Unloaded nanoparticles and free BC in solution (7µg/mL; Fig. S3) were used as controls. First, the minimal inhibitory concentration of BC was evaluated using the Kirby-Bauer disc diffusion method for testing microbial susceptibility to new antibiotic drugs was used [38]. Briefly, the bacterial cultures were grown overnight at 37 °C with agitation (140 rpm), and their optical density was adjusted to 0.1 (λ= 610 nm; McFarland standard 0.5) to obtain a bacterial inoculum of 10^8 CF/mL. They were spread on Muller Hinton Agar (Oxoid, UK) with a sterile swab. Blank discs were impregnated with 30 µL of each bacitracin solution (0.052, 0.104, 0.208, 0.500, and 0.800 mg/mL). The concentrations of BC were chosen according to the literature available [39]. Negative controls using only sterile PBS were used. The plates were incubated for 16 h at 37 °C. The area of growth inhibition was calculated by measuring the diameter of the halo formed around the disks.

The agar well diffusion method was employed as an adaptation of the Kirby-Bauer disc diffusion technique for testing microbial susceptibility to new nanoparticles [38]. This method provides a more reliable assessment of charged substances, which can adhere to the hydrophilic surface of the disc and do not disperse into the surrounding medium [40–42]. The bacterial cultures were grown as previously described above and their optical density was adjusted to 0.1 (λ= 610 nm; McFarland standard 0.5) corresponding to a bacterial inoculum of 10^8 CFU/mL. They were then spread onto Muller Hinton Agar (Oxoid, UK) with a sterile swab. Four wells (4 mm diameter) were made with a sterile punch and 30 µL of each nanoparticle suspension was added to each well [40–42]. Negative control with PBS and positive control with BC solution were used. The plates were incubated for 48 h at 25 °C and for 16 h at 37 °C. The growth inhibition was determined by measuring the diameter of the halo formed around the disks [43,44]. All experiments were performed in triplicates to ensure reproducibility.

2.7.2 Bacterial viability in liquid media

The viability of Gram-positive bacteria in the presence of the BC-loaded HAMA/CS-Xlinked nanoparticles was assessed against *S. aureus*, MRSA, and *S. epidermidis* [45]. Before the experimental work, all the nanoparticles were produced in sterilized conditions. Bacterial cultures were grown overnight in Tryptone Soya Broth (TSB; Oxoid, UK) medium at 37 ºC overnight with agitation (150 rpm) and adjusted to an optical density of 0.1 (λ = 610 nm). A volume of 60 µL of the bacterial suspensions was added to 60 µL of 2 x concentrated HAMA/CS-Xlinked nanoparticles and BC-loaded HAMA/CS-Xlinked nanoparticles. 60 µL of BC solution (0.7 mg/ml) was used as positive control and 60 µL of sterile PBS as negative control. Samples were incubated at 37 ºC under static conditions for 24 h and 72 h. After each timepoint, serial dilutions were made, spread onto Tryptone Soya Agar (TSA; Oxoid, UK), and incubated overnight at 37 ºC. The bacterial viability was determined as the log the colony forming units (CFU/mL). Each experiment was performed in triplicate at two consecutive times.

2.8. Antibiofilm activity of the BC-Loaded HAMA/CS-Xlinked nanoparticles

The antibiofilm activity of the BC-loaded HAMA/CS-Xlinked nanoparticles was assessed against *S. aureus*, MRSA, and *S. epidermidis* using the microtiter plate method according to Haney *et al.* [46]. A bacterial biofilm was first established for all the strains in 96-well plates. Bacterial cultures were grown overnight in TSB medium at 37ºC with agitation (150 rpm) and 100 µl of each bacterial suspension adjusted to an optical density of 0.1 (λ = 610 nm) was added to the 96-well plate and incubated for 16 h at 37 °C under static conditions. After incubation, gently rinse the adhered biofilms with sterile PBS, following by aspirating the rinsing media and discard it. Then, 60 µl of 2 x concentrated solution of HAMA/CS-Xlinked nanoparticles, BC-loaded HAMA/CS-Xlinked nanoparticles, BC in solution and of sterile TSB were added in triplicate to each well containing the biofilm. Plates were incubated for 24 h and 72 h under static conditions at 37 ºC. The bacterial recoverable from the biofilm after each treatment was determined as the log the colony forming units (CFU/mL). As for biofilm formation, it was quantified using Crystal Violet method[46]. Briefly, after incubation, 96-well plates were washed with sterile PBS three times to remove planktonic bacteria and leave plate to dry. Then, adherent bacterial cells were fixed with 100 % methanol for 20 min and stained with crystal violet (0.1 % w/v) for 20 min. Afterwards, each well was washed twice with PBS, and bound crystal violet was released by adding 33 % (vol/vol) acetic acid. The OD of the resulting solution was measured at 595 nm using a microplate reader (BIO-TEK instruments). Each experiment was performed in triplicate at two consecutive times.

2.9. Biological assays

In vitro cellular tests of the HAMA/CS-Xlinked and BC-loaded HAMA/CS-Xlinked nanoparticles were made with L929 mouse fibroblast cells cultured in DMEM culture medium supplemented with 10 % of FBS and 1 % of Antibiotic-Antimycotic solution [47–49]. The cells were grown in a T150 flask and incubated at 37 °C in a humidified air atmosphere of 5 % CO_2. When 80 % of confluence was reached, the cells were washed with DPBS and subsequently detached with 5 mL of trypLE™ express solution for 5 min at 37 °C. To inactivate the trypLE™ express solution effect, 10 mL of culture medium was added. The cells were centrifuged at 300 x g for 5 min and the medium was removed. The pellet was resuspended in the culture medium. Cellular seeding was performed on nanoparticles produced in sterilized conditions and resuspended with DMEM medium. 20 µL of supplemented DMEM containing a cell

suspension with a density of 30,000 cells was added dropwise carefully above the surface of the culture plate. Tissue culture polystyrene surface (TCPS) with only cells was used as positive control. All experiments were made in triplicate and incubated at 37 °C in a humidified air atmosphere of 5 % CO_2.

The metabolic activity of HAMA/CS-Xlinked and BC-loaded HAMA/CS-Xlinked nanoparticles were determined using the Alamar-Blue assay [47–49]. After 1 and 3 days of culture, the culture medium was removed and the cells were washed twice with sterile PBS (pH 7.4). Then, fresh medium supplemented with 10 % of Alamar-blue reagent (Xpert Blue Cell Viability Assay, GRISP) was added to the culture wells, followed by incubation at dark for 4 h at 37 ºC in a humidified air atmosphere of 5 % CO_2. Afterwards, 100 µL of each solution was transferred to a 96-well black plate and the absorbance was measured at 570 nm excitation wavelength and at 600 nm emission wavelength as a reference control, using a microplate reader (BIO-TEK instruments). The experiments were run in triplicate.

Cell proliferation was evaluated by dsDNA picogreen quantification (P11495, Invitrogen), according to the manufacturer's instructions [47–49]. After each incubation time, DMEM medium was removed from each well and the cells were washed twice with sterile PBS (pH 7.4). Then, 1 mL of ultrapure water was added to each well to induce complete membrane lysis, incubated at 37 °C for 1 h and stored at −80 °C until further analysis. After thawing, samples were analyzed for DNA content and measured at an excitation wavelength of 485/20 nm and at an emission wavelength of 528/20 nm. DNA content was calculated according to a standard curve. The experiments were run in triplicate.

The cell viability of HAMA/CS-Xlinked and BC-loaded HAMA/CS-Xlinked nanoparticles were determined by live/dead assay (Calcein AM stains the live cells in green and PI stains dead cells in red) L929 mouse fibroblast cells were used to assess the viability of HAMA/CS-Xlinked and BC-loaded HAMA/CS-Xlinked nanoparticles [47–49]. After 1 and 3 days of culture, the culture medium was removed and a fresh medium supplemented with 0.2 % Calcein AM and 0.1 % PI were added to immerse the seeded nanoparticles. These immersions lasted for 30 min in the dark and were then washed with DPBS and analyzed using an inverted incubation microscope with Thunder (DMi8, Leica, Germany).

2.10. Statistical Analysis of the Obtained Data

All the quantitative results were obtained from triplicate samples. Data are reported as mean ± standard deviation and tested for normality. Significant statistical variations were calculated by One-way ANOVA with Tukey tests to compare between more than two groups; and Two-way ANOVA with Bonferroni tests to compare between more than two groups (GraphPad Prism 9, San Diego CA, USA). The levels of significance for statistical differences are presented as $p < 0.05$(*), $p < 0.01$(**), and $p < 0.001$(***).

3. Results and discussion

3.1. Synthesis and characterization of HAMA

In order to obtain HAMA, a well-established method of HA methacrylation by reaction with methacrylic anhydride was used (Fig. 1A) [31]. The modification was confirmed by ^{1}H-NMR (Fig. 1B), which revealed new signals at 5.7 ppm and 6.2 ppm for the protons of vinyl groups, and at 1.9 ppm for the methyl protons (Fig. 1B and Fig. S1)[31]. The degree of methacrylation was 20 %, as calculated from the ratio of the integral of the HA methyl proton (peak at 2.0 ppm) to the HAMA methyl proton (peak at 1.9 ppm).

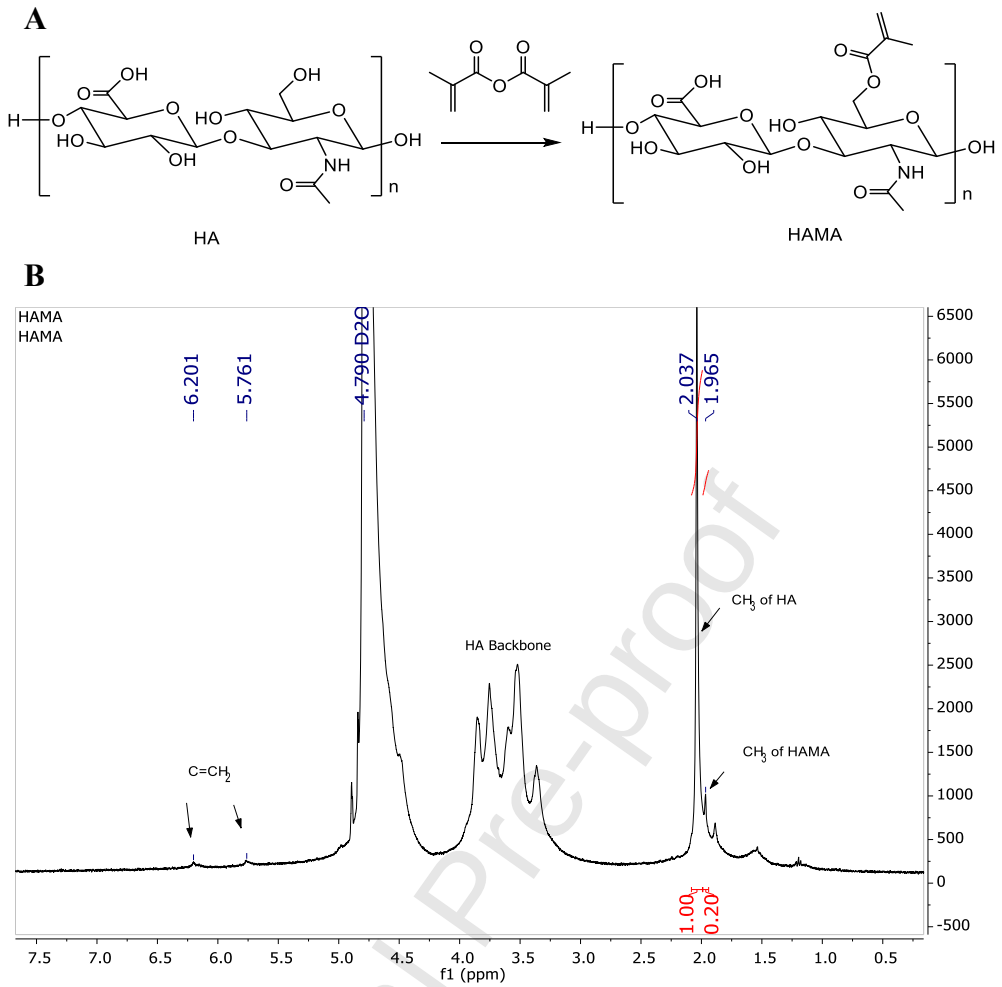

Fig. 1 (A) Schematic presentation of the chemical reaction used for the methacrylation of hyaluronic acid (HA) and (B) ^{1}H-NMR spectrum of the obtained methacrylated hyaluronic acid (HAMA).

3.2. Assembly and Characterization of Nanoparticles

The CS and HA used in this study are appealing materials not only because of their benefits in the pharmaceutical industry but also because they exhibit ionizable amine and carboxyl groups, which allow their complexation by electrostatic interactions [50]. The nanoparticles were obtained by mixing CS with HA or HAMA at room temperature. DLS measurements showed that nanoparticles assembled from HA/CS and HAMA/CS have similar diameters of 742 and 769 nm, respectively (Fig. 2A and Table 1). However, they showed high polydispersity (PDI > 0.37) indicating instability and/or aggregation. So, an additional modification via cross-linking was made. HAMA/CS-Xlinked nanoparticles had a smaller diameter (478 nm) and lower polydispersity (PDI =

0.30, consistent with a more uniform distribution) [51]. As expected, the nanoparticles were negatively charged due to the non-stoichiometric ratio of the used components, *i.e.* HA was used in excess compared to CS [52]. The zeta potentials were approximately -30 mV, indicating that the suspended nanoparticles retain colloidal stability[53]. Scanning electron microscopy (SEM) confirmed the data from DLS by showing the formation of nanoparticles with spherical shape (Fig. 2B and Fig. S2).

Different times of UV irradiation, namely 15, 30, 45 and 60 sec were tested, but there was no change in the size of the nanoparticles produced (Table S1).

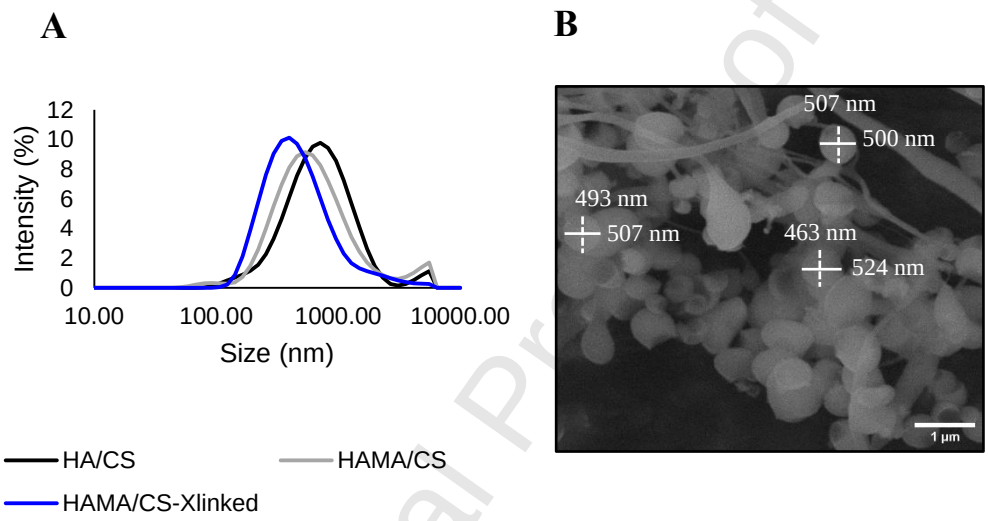

Fig. 2 (A) Dynamic light scattering (DLS) data showing the size distribution on nanoparticle samples. Representative spectra are represented. Peaks around 10 000 nm are attributed to NP aggregates (low signal, ≈1% intensity). (B) Representative scanning electron microscopy image of crosslinked nanoparticles.

Table 1 DLS data for size, polydispersity and charge of the obtained nanoparticles.

Formulation	Size (nm)	PDI	Zeta potential (mV)
HA/CS	769±69	0.373±0.068	-35.8±0.2
HAMA/CS	742±231	0.410±0.054	-32.5±0.6
HAMA/CS-Xlinked	478±86	0.300±0.074	-29.2±1.1

3.3. Nanoparticle Stability

The stability of nanoparticles is an important factor to determine their efficacy as a delivery system and is related to the tendency of nanoparticulate formulations to aggregate or degrade overtime [54]. To this end, the hydrodynamic diameters and PDI values of our systems were evaluated during 14 days as an indicator of their stability (Fig. 3). The selected temperatures of 25 °C and 37 °C correspond to the temperature

range where the systems will be used: room temperature (on the wound surface) and physiological temperature (when in contact with the tissue).

Since the pH of chronic wounds is in the range between 7.2–8.9 [55], a medium with an acidic pH (≈5) was chosen. This pH is relevant because an acidic microenvironment reduces the proteolytic activity and bacteria growth that is associated with slow wound healing [56]. In fact, the use of acidic substances has been proposed to accelerate wound healing and restore the acidic pH of the skin milieu[57–59]. HAMA/CS-Xlinked nanoparticles were systematically smaller than HA/CS and HAMA/CS at all time-points as a result of the increased crosslinking density (without crosslinked 769 and 742 nm, respectively and with crosslinked 478 nm). Size is an important aspect to consider when designing drug delivery systems: because particle size is inversely proportional to their diffusion coefficient, smaller particles have higher effective encapsulated doses and are better distributed in tissues [60,61].

Regardless of the composition, at these conditions, the size and PDI of HA/CS and HAMA/CS nanoparticles did not change significantly during the studied period of 14 days. The HAMA/CS-Xlinked nanoparticles remained homogenous (*i.e.*, PDI < 0.3) and with a diameter below 500 nm but these parameters decreased significantly at 25 °C during the studied period. These data suggest that the crosslinked nanoparticles become more compact over time as the low PDI discards the possibility of nanoparticle fragmentation - an opposite trend would indicate degradation or aggregation [62,63]. At 37 °C, no significant variations of size or PDI were found, indicating nanoparticle stability at these conditions.

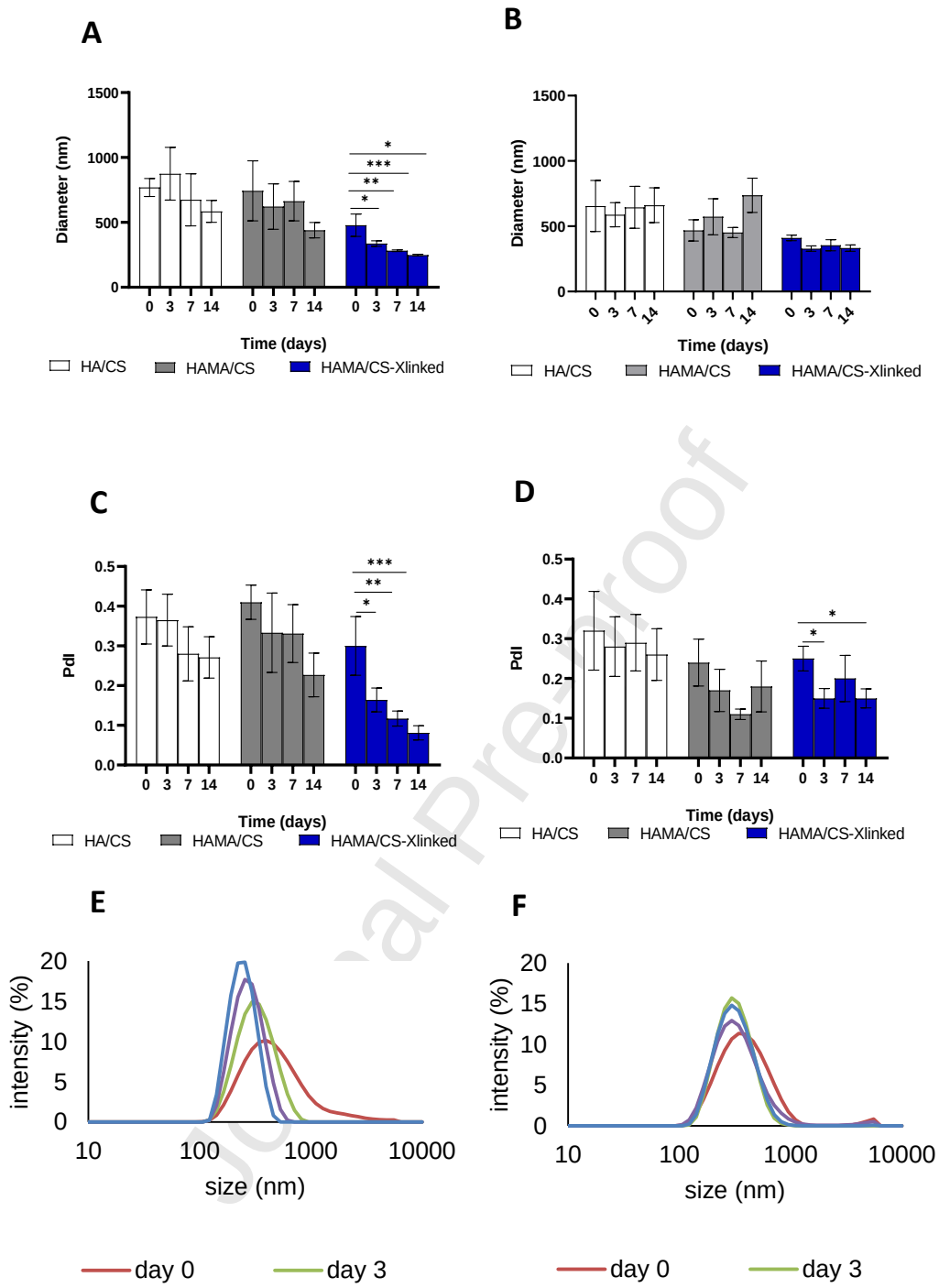

Fig. 3 Dynamic light scattering (DLS) data showing the size variations of nanoparticles samples at 25 °C (A) and 37 °C (B). PDI variations of nanoparticles samples at 25 °C (C) and 37 °C (D). Size distribution evolution of HAMA/CS-Xlinked nanoparticles at 25 °C (E) and 37 °C (F).

3.4. Encapsulation of Bacitracin

BC, an antibiotic used to treat of wounds, is most effective against gram-positive bacteria [64]. In this study, different concentrations of BC (> 0.052 mg/mL) were tested (Fig. S3 and Table S2). The results show that BC had an inhibitory effect at concentrations greater than 0.5 mg/mL on all the bacteria tested, which is consistent with previous studies [65]. To endow the HAMA/CS-Xlinked nanoparticles with antibacterial properties, BC was encapsulated at 0.7 mg/mL. The encapsulation efficiency was 97 %, as determined by analytical HPLC (Fig. S4), and it affected the dimensions of this system: the obtained BC-loaded nanoparticles had a diameter of 332 nm (lower than the 478 nm of unloaded HAMA/CS-Xlinked) with a PDI of 0.256 (Fig. 4).

The decrease in the size of BC-loaded HAMA/CS-Xlinked nanoparticles can be explained by the interaction of CS with BC. Through ^{1}H-NMR analysis (Fig. 4C) it is possible to verify a deviation chemical shift in the spectrum of CS more BC, suggesting a chemical interaction between them.

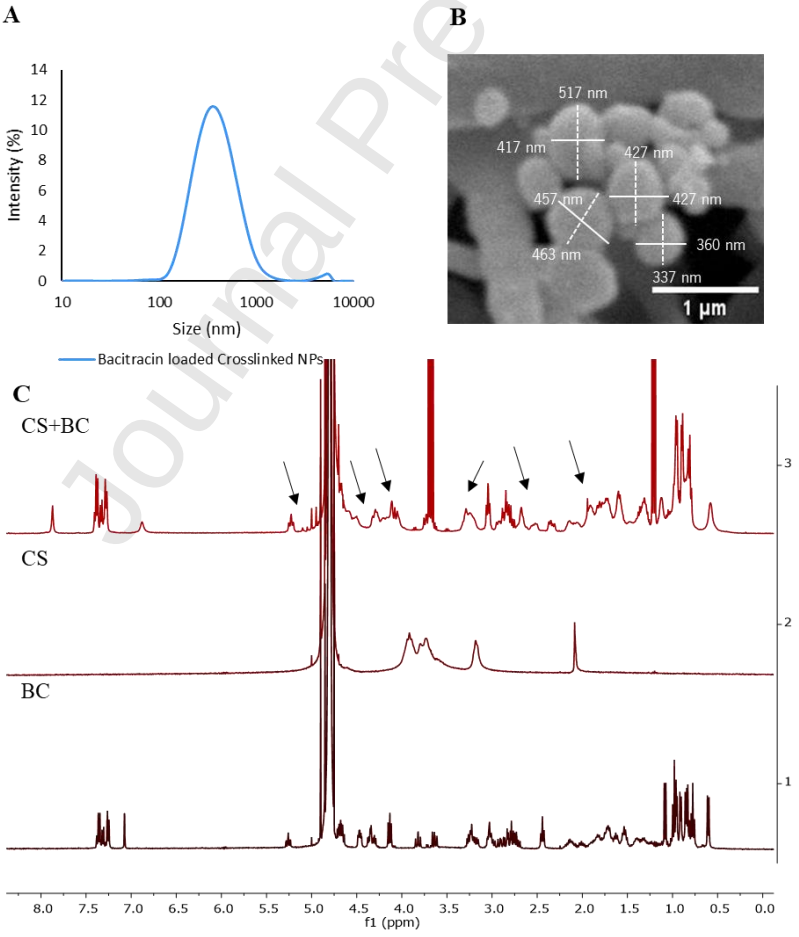

Fig. 4 (A) Size distribution on BC-loaded HAMA/CS-Xlinked nanoparticles. (B) SEM imaging of BC-loaded HAMA/CS-Xlinked nanoparticles, with diameter measurements. (C) ^{1}H-NMR spectra (400MHz, D_2O) of BC, CS, and CS+BC.

3.5. Antibacterial Potential of Loaded Nanoparticles

The antibacterial activity of BC-loaded HAMA/CS-Xlinked nanoparticles was evaluated at 25 and 37 °C against three gram-positive bacteria: *S. aureus*, MRSA, and *S. epidermidis* (Fig. 5 and Fig. S5) according to the modified agar-well Kirby–Bauer plate method [35]. Because the diffusion of nanoparticles is inversely proportional to their size [60,61], a good spreading of loaded nanoparticles within the agar matrix was anticipated. At 25 °C, unloaded HAMA/CS-Xlinked nanoparticles had no antibacterial effect, but BC-loaded nanoparticles were effective against *S. aureus* (Fig. 5A, Table 2). Plates inoculated with *S. aureus*, MRSA, and *S. epidermidis* showed a clear inhibition zone around the positive control containing BC solution after incubation at 25 °C.

When incubated at 37 ºC, the loaded nanoparticles had an antibacterial effect against all studied strains, as evidenced by the clear inhibition zone formed on all tested bacteria cultures (between 11 and 15 mm in diameter) (Fig. 5B, Table 2).

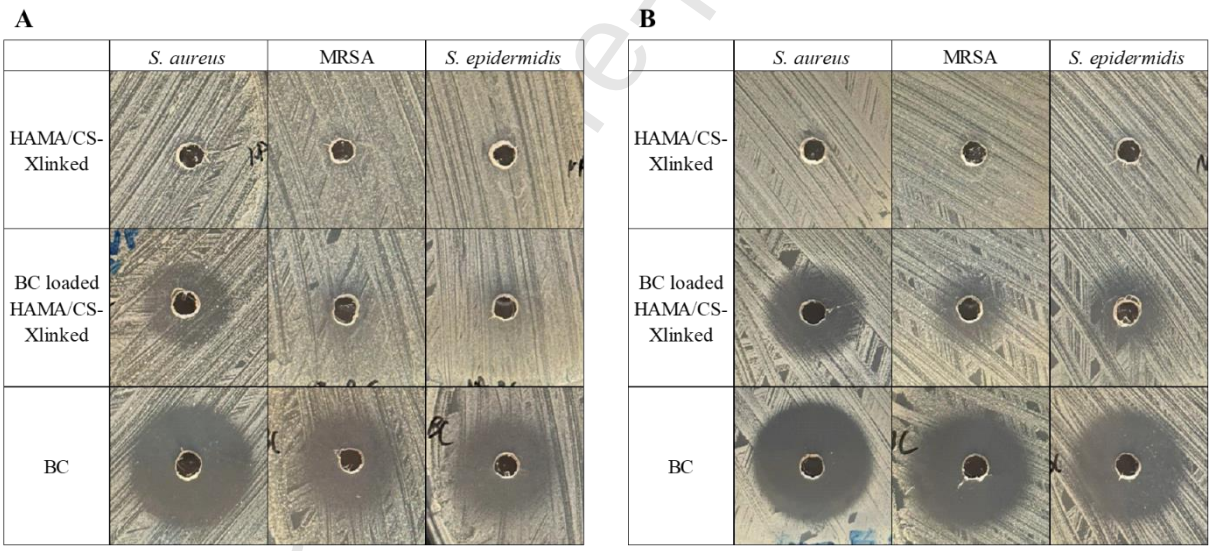

Fig. 5 Representative image of the antibacterial activity of HAMA/CS-Xlinked nanoparticles, BC-loaded HAMA/CS-Xlinked nanoparticles, and BC against *S. aureus*, MRSA, *S. epidermidis* using agar well diffusion assay at 25 °C (A) and 37 °C (B).

Table 2 Qualitative data (diameter of inhibition zones) about the antibacterial effect of different formulations.

Temperature	Formulation	Diameter of the inhibition zone [mm]		
		S. aureus	MRSA	*S. epidermidis*
25 °C	HAMA/CS-Xlinked	0	0	0
	BC-loaded HAMA/CS-Xlinked	14	5	5
	BC	20	16	17
37 °C	HAMA/CS-Xlinked	0	0	0
	BC-loaded HAMA/CS-Xlinked	15	11	11
	BC	19	19	19

Although the BC-loaded HAMA/CS-Xlinked nanoparticles showed a lower inhibition effect at 25 °C, the results suggest that this formulation can be used in a variety of strategies to prevent the proliferation of the most common microorganisms responsible for wound infection [66,67]. The encapsulation of BC is advantageous for its administration since its effects would be stronger when in direct contact with the wound bed, at temperatures closer to 37 °C.

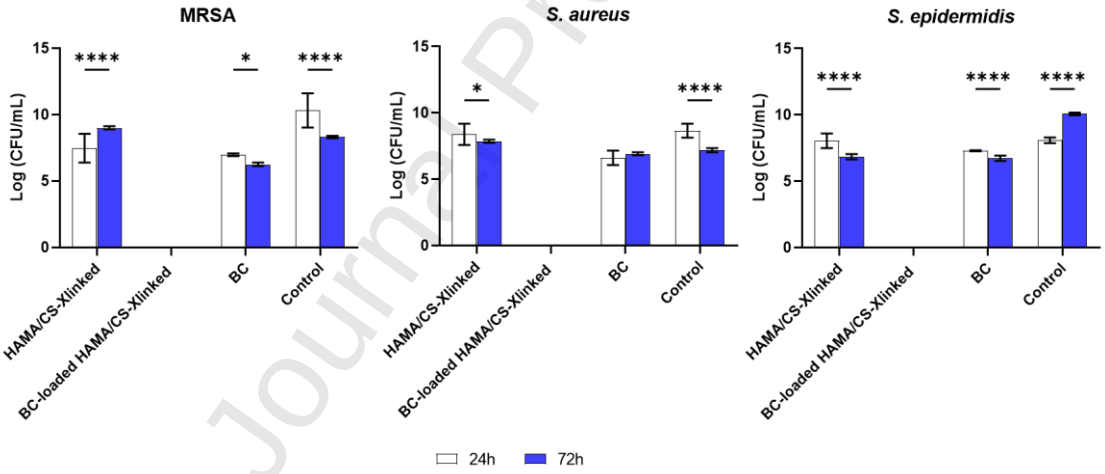

Fig. 6 Activity of HAMA/CS-Xlinked and BC-loaded HAMA/CS-Xlinked nanoparticles, and BC in solution against *MRSA*, *S. aureus*, and *S. epidermidis* after 24 h and 72 h incubation. Number of recoverable bacteria was evaluated by log (CFU/mL). Control corresponds to the bacteria without any treatment.

The effect of the BC-loaded HAMA/CS-Xlinked nanoparticles on bacterial viability was evaluated (Fig. 6). The results show that the BC-loaded HAMA/CS-Xlinked nanoparticles had a bacterial inhibitory effect for all strains after 24 h incubation (Fig. 6). The same trend was observed in the bacteria treated with BC in solution (Fig. 6). As for the HAMA/CS-Xlinked nanoparticles, they had no effect on the

bacterial growth, demonstrating a similar pattern to the bacterial controls without any treatment. The HAMA/CS-Xlinked nanoparticles exhibited no impact on bacterial growth, displaying a comparable trend to the untreated bacterial controls. Following a 72 h incubation period, a similar pattern was seen, suggesting that the HAMA/CS-linked nanoparticles loaded with BC exhibit a potent antibacterial action.

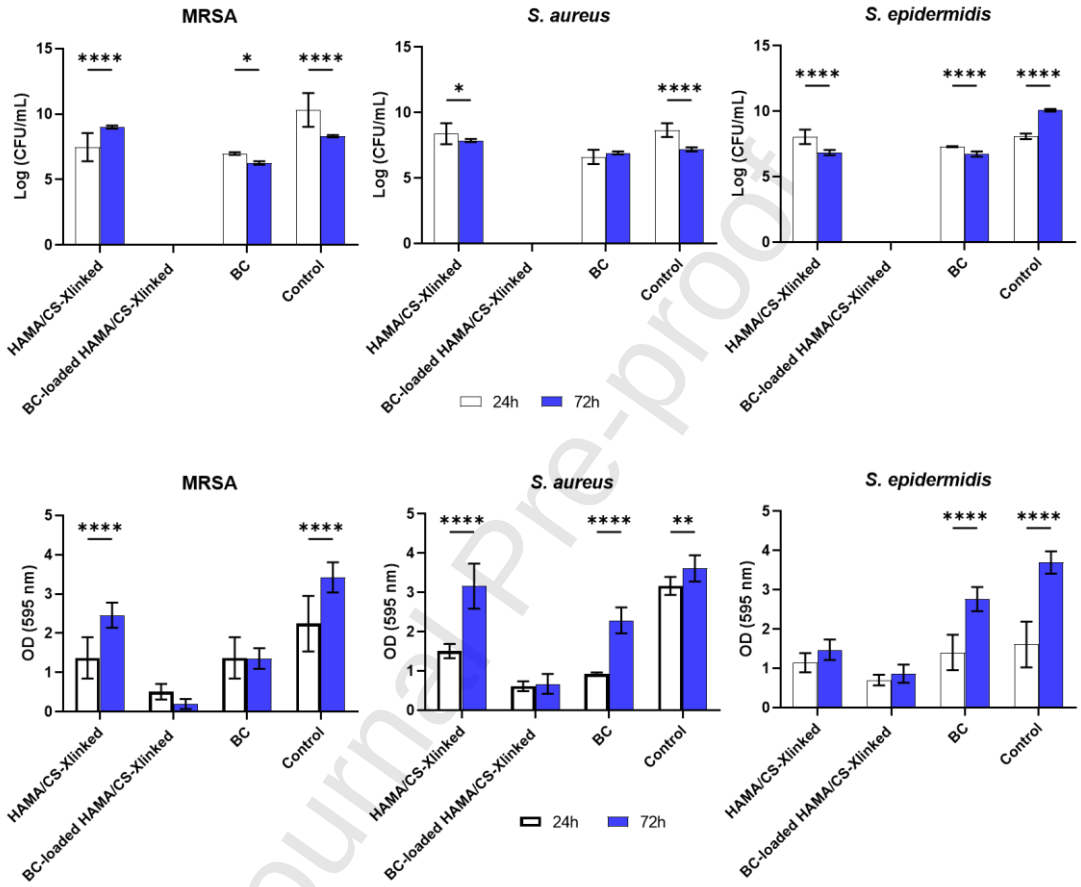

Fig. 7 Antibiofilm activity of the HAMA/CS-Xlinked and BC-loaded HAMA/CS-Xlinked nanoparticles, and BC in solution against *MRSA*, *S. aureus*, and *S. epidermidis* after 24 h and 72 h incubation. Control corresponds to the bacteria without any treatment. Biofilm was determined by: (A) Number of recoverable bacteria was evaluated by Log (CFU/mL), and (B) Biofilm biomass formation using the Crystal Violet assay. Significant differences: **p < 0.01,****p < 0.0001.

The antibiofilm potential of the BC-loaded HAMA/CS-Xlinked nanoparticles was also evaluated using the microtiter plate method (Fig. 7A). Following incubation periods of 24 h and 72 h, the results indicate that no viable bacteria were detected when exposed to the BC-loaded HAMA/CS-Xlinked nanoparticles. However, the growth and production of biofilm were not affected by HAMA/CS-Xlinked nanoparticles or BC in solution, indicating that they did not hinder these processes. Similar patterns were noted

in relation to the biofilm biomass, as depicted in Fig. 7B. The results suggest that the BC-loaded HAMA/CS-Xlinked nanoparticles reduced the amount of biofilm after 24 h and 72 h of incubation, in comparison to the bacteria treated with HAMA/CS-Xlinked nanoparticles and those that received no treatment. This occurrence was detected in all the bacteria that were examined. After 72 h of incubation, the antibacterial ability of the BC-loaded HAMA/CS-Xlinked NPs was further demonstrated.

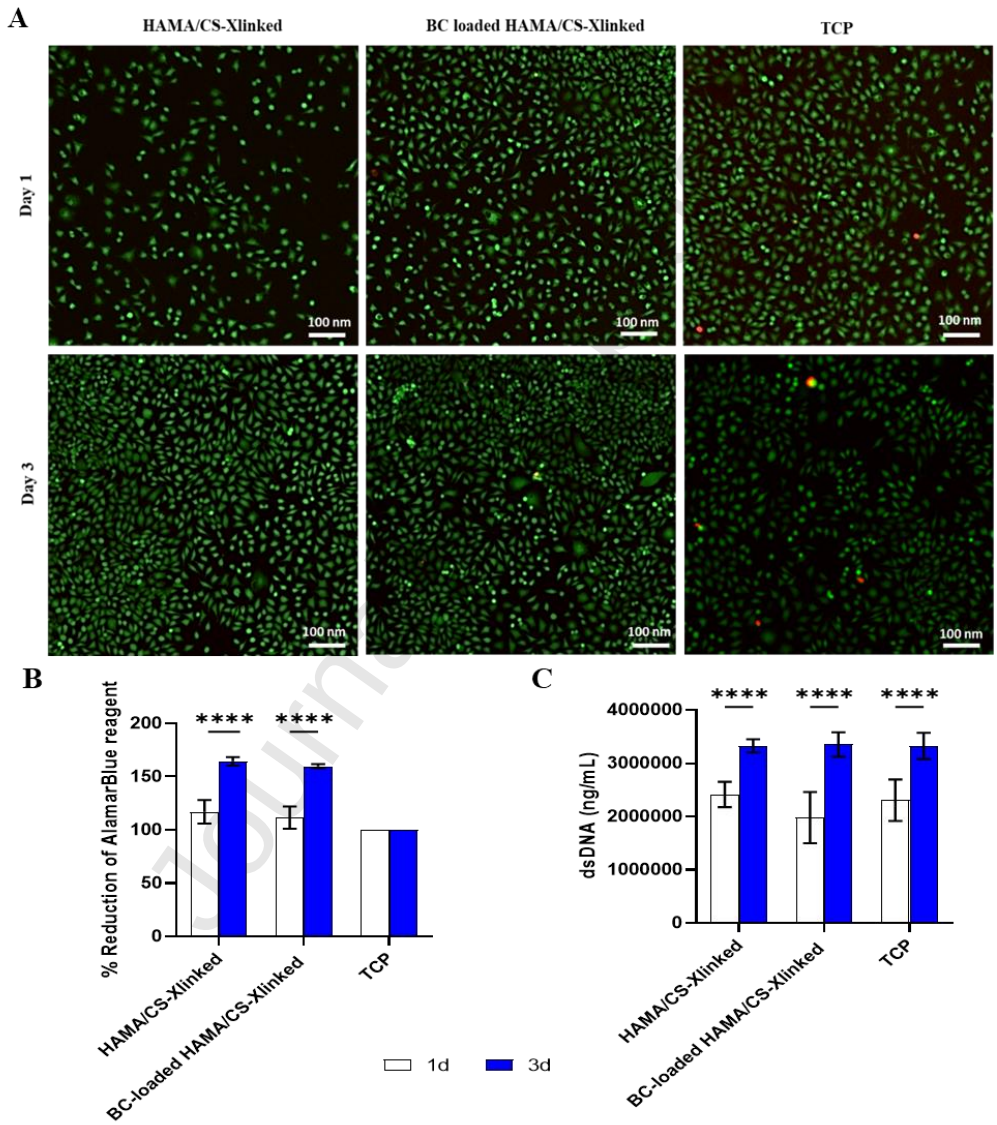

Fig. 8 (A) Representative fluorescent images of live (green)/dead (red) cells on the HAMA/CS-Xlinked and the BC-loaded HAMA/CS-Xlinked nanoparticles. Scale bar is 100 μm. (B) Metabolic activity of L929 cells cultured with the HAMA/CS-Xlinked and the BC-loaded HAMA/CS-Xlinked nanoparticles determined by Alamar blue assay. (C) Double strand DNA (dsDNA) quantification assay of L929 cells cultured with the HAMA/CS-Xlinked and the BC-loaded HAMA/CS-Xlinked nanoparticles, after 1 day and 3 days. L929 cells in tissue culture plastic (TCP) were used as a positive control. Significant differences: ****$p < 0.0001$.

The cytotoxic response to the BC-loaded HAMA/CS-Xlinked and HAMA/CS-Xlinked nanoparticles was evaluated using L929. The live/dead assay (Fig. 8A) showed a minimal number of dead cells (in red), showed no cytotoxicity effect. Significant differences in the metabolic activity of cells cultured on HAMA/CS-Xlinked and HAMA/CS-Xlinked nanoparticles were observed on the third day: L929 cultured on BC-loaded HAMA/CS-Xlinked and HAMA/CS-Xlinked NPs represented the similar metabolic activity (Fig. 8B). An increase in DNA content and metabolic activity was observed over time in culture, indicating that the nanoparticles are able to sustain cell proliferation (Fig. 8C).

This antibacterial study showed that BC-loaded HAMA/CS-Xlinked nanoparticles have created novel antibacterial polymers for treating wound infections. These polymers effectively inhibit bacterial growth and prevent biofilm formation, while also promoting cellular growth and proliferation. They can serve as beneficial nanotechnological alternatives for existing conventional topical treatments, delivering antibiotics directly to deep infected wounds [68]. Furthermore, the nanoparticles extensive surface area allows for improved efficacy of drugs, while also somewhat mitigating their toxicity.

4. Conclusions

This work demonstrated the successful production of CS/HAMA nanoparticles for the delivery of BC. The nanoparticles were produced using, for the first time, methacrylated HA to photo-crosslink upon UV irradiation. Cross-linked nanoparticles were found to be smaller and more monodispersed when loaded with BC, measuring around 350 nm, which is useful in the reactive microenvironment of wounds. The obtained nanoparticles are especially promising as topical antibacterial compounds for wound treatments, as demonstrated by the encapsulation of BC: the antibiotic-loaded nanoparticles inhibited the growth of bacterial strains common in diabetic foot ulcers. The proposed methodology is simple, versatile and scalable for industrial production of nanoparticles. The process is both sustainable and cost-effective, as it uses building blocks from renewable sources and does not require specialized equipment or aggressive temperatures or solvent conditions. Furthermore, these nanoparticles demonstrate enhanced antibacterial and antibiofilm effects and are non-cytotoxic on fibroblasts. While a comparison with other wound healing therapies was not contemplated, the efficacy of the proposed system can be tested against *in vitro* and *in*

vivo models in future experiments to assess clinical applicability. The focus is envisaged to be on chronic wound therapies, as these wounds are challenging to treat and are often associated with underlying complications prevalent in modern societies.

Acknowledgements

The authors acknowledge the financial support of the European Commission through project APTADEGRAD (HORIZON-EIC-2022-PATHFINDEROPEN-01-101099063). The authors acknowledge the SHIFT Project, funded by the European Union's Horizon 2020 Research and Innovation programme under the Maria Sklodowska-Curie grant agreement no. 101008041. R.R.G. acknowledges the Erasmus Program for the travel grant to the University of Trento. R.R.C. acknowledges FCT for support through grant 2022.00764.CEECIND/CP1718/CT0020 (https://doi.org/10.54499/2022.00764.CEECIND/CP1718/CT0020). A.R.F acknowledges FCT for support through grant DL 57/2016/CP1377/CT0054 (https://doi.org/10.54499/DL57/2016/CP1377/CT0054) and PTDC/BTM-MAT/2844/2021 (https://doi.org/10.54499/PTDC/BTM-MAT/2844/2021) funded by the Portuguese National Science Foundation (FCT) through OE component. The authors would like to thank the contributions to this research from the project "TERM RES Hub – Scientific Infrastructure for Tissue Engineering and Regenerative Medicine", reference PINFRA/22190/2016 (Norte-01-0145-FEDER-022190), funded by the Portuguese National Science Foundation (FCT) in cooperation with the Northern Portugal Regional Coordination and Development Commission (CCDR-N), for providing relevant lab facilities, state-of-the art equipment and highly qualified human resources.

References

[1] R.G. Frykberg, J. Banks, Challenges in the Treatment of Chronic Wounds, Adv Wound Care (New Rochelle) 4 (2015) 560–582. https://doi.org/10.1089/wound.2015.0635.

[2] G. Broughton, J.E. Janis, C.E. Attinger, The basic science of wound healing, Plast Reconstr Surg 117 (2006). https://doi.org/10.1097/01.prs.0000225430.42531.c2.

[3] R.G. Frykberg, J. Banks, Challenges in the Treatment of Chronic Wounds, Adv Wound Care (New Rochelle) 4 (2015) 560–582. https://doi.org/10.1089/wound.2015.0635.

[4] S. Guo, L.A. DiPietro, Critical review in oral biology & medicine: Factors affecting wound healing, J Dent Res 89 (2010) 219–229. https://doi.org/10.1177/0022034509359125.

[5] C.K. Sen, G.M. Gordillo, S. Roy, R. Kirsner, L. Lambert, T.K. Hunt, F. Gottrup, G.C. Gurtner, M.T. Longaker, Human skin wounds: A major and snowballing threat to public health and the economy: PERSPECTIVE ARTICLE, Wound Repair and Regeneration 17 (2009) 763–771. https://doi.org/10.1111/j.1524-475X.2009.00543.x.

[6] M. Holl, J.; Kowalewski, C.; Zimek, Z.; Fiedor, P.; Kaminski, A.; Oldak, T.; Moniuszko, Chronic Diabetic Wounds and Their Treatment with Skin Substitutes, Cells 10 (2021). https://doi.org/https://doi.org/10.3390/cells 10030655.

[7] A. Alavi, R.G. Sibbald, D. Mayer, L. Goodman, M. Botros, D.G. Armstrong, K. Woo, T. Boeni, E.A. Ayello, R.S. Kirsner, Diabetic foot ulcers: Part II. Management, J Am Acad Dermatol 70 (2014) 21.e1-21.e24. https://doi.org/10.1016/j.jaad.2013.07.048.

[8] R. Stein-Wexler, Musculoskeletal infection, 2015. https://doi.org/10.1007/978-3-642-45381-6_19.

[9] F. Gottrup, A specialized wound-healing center concept: Importance of a multidisciplinary department structure and surgical treatment facilities in the treatment of chronic wounds, Am J Surg 187 (2004) S38–S43. https://doi.org/10.1016/S0002-9610(03)00303-9.

[10] K. Järbrink, G. Ni, H. Sönnergren, A. Schmidtchen, C. Pang, R. Bajpai, J. Car, Prevalence and incidence of chronic wounds and related complications: A protocol for a systematic review, Syst Rev 5 (2016) 1–6. https://doi.org/10.1186/s13643-016-0329-y.

[11] J. Tan, S. Shah, A. Thomas, H.D. Ou-Yang, Y. Liu, The influence of size, shape and vessel geometry on nanoparticle distribution, Microfluid Nanofluidics 14 (2013) 77–87. https://doi.org/10.1007/s10404-012-1024-5.

[12] J.W. Hickey, J.L. Santos, J.M. Williford, H.Q. Mao, Control of polymeric nanoparticle size to improve therapeutic delivery, Journal of Controlled Release 219 (2015) 536–547. https://doi.org/10.1016/j.jconrel.2015.10.006.

[13] M.J. Mitchell, M.M. Billingsley, R.M. Haley, M.E. Wechsler, N.A. Peppas, R. Langer, Engineering precision nanoparticles for drug delivery, Nat Rev Drug Discov 20 (2021) 101–124. https://doi.org/10.1038/s41573-020-0090-8.

[14] R.R. Costa, R.L. Reis, I. Pashkuleva, Glycosaminoglycans as polyelectrolytes: implications in bioactivity and assembly of biomedical devices, International Materials Reviews 67 (2022) 765–795. https://doi.org/10.1080/09506608.2022.2026860.

[15] I. Aranaz, A.R. Alcántara, M.C. Civera, C. Arias, B. Elorza, A.H. Caballero, N. Acosta, Chitosan: An overview of its properties and applications, Polymers (Basel) 13 (2021). https://doi.org/10.3390/polym13193256.

[16] N. Morin-crini, E. Lichtfouse, G. Torri, G. Crini, N. Morin-crini, E. Lichtfouse, G. Torri, G.C. Fundamentals, N. Morin-crini, E. Lichtfouse, G. Torri, G. Crini, Fundamentals and Applications of Chitosan To cite this version : HAL Id : hal-02152878 Fundamentals and Applications of Chitosan, Springer International Publishing AG, 2019.

[17] W. Xia, P. Liu, J. Zhang, J. Chen, Biological activities of chitosan and chitooligosaccharides, Food Hydrocoll 25 (2011) 170–179. https://doi.org/10.1016/j.foodhyd.2010.03.003.

[18] S. (Gabriel) Kou, L. Peters, M. Mucalo, Chitosan: A review of molecular structure, bioactivities and interactions with the human body and micro-organisms, Carbohydr Polym 282 (2022) 119132. https://doi.org/10.1016/j.carbpol.2022.119132.

[19] A. Fallacara, E. Baldini, S. Manfredini, S. Vertuani, Hyaluronic acid in the third millennium, Polymers (Basel) 10 (2018). https://doi.org/10.3390/polym10070701.

[20] A. Yasin, Y. Ren, J. Li, Y. Sheng, C. Cao, K. Zhang, Advances in Hyaluronic Acid for Biomedical Applications, 10 (2022) 1–12. https://doi.org/10.3389/fbioe.2022.910290.

[21] Y. Parajó, I. D'Angelo, A. Welle, M. Garcia-Fuentes, M.J. Alonso, Hyaluronic acid/Chitosan nanoparticles as delivery vehicles for VEGF and PDGF-BB, Drug Deliv 17 (2010) 596–604. https://doi.org/10.3109/10717544.2010.509357.

[22] A. Tirella, K. Kloc-Muniak, L. Good, J. Ridden, M. Ashford, S. Puri, N. Tirelli, CD44 targeted delivery of siRNA by using HA-decorated nanotechnologies for KRAS silencing in cancer treatment, Int J Pharm 561 (2019) 114–123. https://doi.org/10.1016/j.ijpharm.2019.02.032.

[23] E. Lallana, J.M. Rios De La Rosa, A. Tirella, M. Pelliccia, A. Gennari, I.J. Stratford, S. Puri, M. Ashford, N. Tirelli, Chitosan/Hyaluronic Acid Nanoparticles: Rational Design Revisited for RNA Delivery, Mol Pharm 14 (2017) 2422–2436. https://doi.org/10.1021/acs.molpharmaceut.7b00320.

[24] L. Yang, S. Gao, S. Asghar, G. Liu, J. Song, X. Wang, Q. Ping, C. Zhang, Y. Xiao, Hyaluronic acid/chitosan nanoparticles for delivery of curcuminoid and its in vitro evaluation in glioma cells, Int J Biol Macromol 72 (2015) 1391–1401. https://doi.org/10.1016/j.ijbiomac.2014.10.039.

[25] A.C. Lima, R.L. Reis, H. Ferreira, N.M. Neves, Cellular Uptake of Three Different Nanoparticles in an Inflammatory Arthritis Scenario versus Normal Conditions, Mol Pharm 18 (2021) 3235–3246. https://doi.org/10.1021/acs.molpharmaceut.1c00066.

[26] O.Z. Fisher, N.A. Peppas, Polybasic nanomatrices prepared by UV-initiated photopolymerization, Macromolecules 42 (2009) 3391–3398. https://doi.org/10.1021/ma801966r.

[27] D.C. Forbes, N.A. Peppas, Polycationic nanoparticles for siRNA delivery: Comparing ARGET ATRP and UV-initiated formulations, ACS Nano 8 (2014) 2908–2917. https://doi.org/10.1021/nn500101c.

[28] S. Maiz-Fernández, L. Pérez-Álvarez, U. Silván, J.L. Vilas-Vilela, S. Lanceros-Mendez, Photocrosslinkable and self-healable hydrogels of chitosan and hyaluronic acid, Int J Biol Macromol 216 (2022) 291–302. https://doi.org/10.1016/j.ijbiomac.2022.07.004.

[29] S. Maiz-Fernández, N. Barroso, L. Pérez-Álvarez, U. Silván, J.L. Vilas-Vilela, S. Lanceros-Mendez, 3D printable self-healing hyaluronic acid/chitosan polycomplex hydrogels with drug release capability, Int J Biol Macromol 188 (2021) 820–832. https://doi.org/10.1016/j.ijbiomac.2021.08.022.

[30] O.Z. Fisher, T. Kim, S.R. Dietz, N.A. Peppas, Enhanced core hydrophobicity, functionalization and cell penetration of polybasic nanomatrices, Pharm Res 26 (2009) 51–60. https://doi.org/10.1007/s11095-008-9704-2.

[31] E. Tous, J.L. Ifkovits, K.J. Koomalsingh, T. Shuto, T. Soeda, N. Kondo, J.H. Gorman, R.C. Gorman, J.A. Burdick, Influence of injectable hyaluronic acid hydrogel degradation behavior on infarction-induced ventricular remodeling, Biomacromolecules 12 (2011) 4127–4135. https://doi.org/10.1021/bm201198x.

[32] R. Nguyen, N. R. Khanna, A. O. Safadi, Y. Sun, Bacitracin Topical, 2022.

[33] C. Loebel, C.B. Rodell, M.H. Chen, J.A. Burdick, Therapeutics and for 3D-Printing, 12 (2020) 1521–1541. https://doi.org/10.1038/nprot.2017.053.Shear-thinning.

[34] E. Lallana, J.M. Rios De La Rosa, A. Tirella, M. Pelliccia, A. Gennari, I.J. Stratford, S. Puri, M. Ashford, N. Tirelli, Chitosan/Hyaluronic Acid Nanoparticles: Rational Design Revisited for RNA Delivery, Mol Pharm 14 (2017) 2422–2436. https://doi.org/10.1021/acs.molpharmaceut.7b00320.

[35] L. Othman, A. Sleiman, R.M. Abdel-Massih, Antimicrobial activity of polyphenols and alkaloids in middle eastern plants, Front Microbiol 10 (2019). https://doi.org/10.3389/fmicb.2019.00911.

[36] C. Luo, M. Chen, K. Luo, X. Yin, M.M. Onchari, X. Wang, J. Zhang, H. Zhong, B. Tian, Genome Sequencing and Genetic Engineering Reveal the Contribution of Bacitracin Produced by Bacillus paralicheniformis CPL618 to Anti-Staphylococcus aureus Activity, Curr Microbiol 80 (2023). https://doi.org/10.1007/s00284-023-03196-1.

[37] King, Allison L, Significance of Open Wounds Potentially Caused by Non-Lethal Weapons, 2019. https://www.researchgate.net/publication/337926082.

[38] L. Othman, A. Sleiman, R.M. Abdel-Massih, Antimicrobial activity of polyphenols and alkaloids in middle eastern plants, Front Microbiol 10 (2019). https://doi.org/10.3389/fmicb.2019.00911.

[39] KnowledgeBASE The antimicrobial index, Bacitracin (Baci-IM), (n.d.). https://antibiotics.toku-e.com/antimicrobial_367_1.html.

[40] M. Bubonja-Šonje, S. Knezević, M. Abram, Challenges to antimicrobial susceptibility testing of plant-derived polyphenolic compounds, Arh Hig Rada Toksikol 71 (2020) 300–311. https://doi.org/10.2478/aiht-2020-71-3396.

[41] C. Valgas, S. Machado De Souza, ; Elza, F.A. Smânia, A. Smânia, SCREENING METHODS TO DETERMINE ANTIBACTERIAL ACTIVITY OF NATURAL PRODUCTS, Brazilian Journal of Microbiology 38 (2007) 369–380.

[42] S. Zheng, M. Bawazir, A. Dhall, H.E. Kim, L. He, J. Heo, G. Hwang, Implication of Surface Properties, Bacterial Motility, and Hydrodynamic Conditions on Bacterial Surface Sensing and Their Initial Adhesion, Front Bioeng Biotechnol 9 (2021). https://doi.org/10.3389/fbioe.2021.643722.

[43] A.R. Franco, E. Palma Kimmerling, C. Silva, F.J. Rodrigues, I.B. Leonor, R.L. Reis, D.L. Kaplan, Silk-Based Antimicrobial Polymers as a New Platform to Design Drug-Free Materials to Impede Microbial Infections, Macromol Biosci 18 (2018) 1–15. https://doi.org/10.1002/mabi.201800262.

[44] J. Hudzicki, Kirby-Bauer Disk Diffusion Susceptibility Test Protocol Author Information, American Society For Microbiology (2012) 1–13.

[45] A.R. Franco, E. Palma Kimmerling, C. Silva, F.J. Rodrigues, I.B. Leonor, R.L. Reis, D.L. Kaplan, Silk-Based Antimicrobial Polymers as a New Platform to Design Drug-Free Materials to Impede Microbial Infections, Macromol Biosci 18 (2018). https://doi.org/10.1002/mabi.201800262.

[46] E.F. Haney, M.J. Trimble, R.E.W. Hancock, Microtiter plate assays to assess antibiofilm activity against bacteria, Nat Protoc 16 (2021) 2615–2632. https://doi.org/10.1038/s41596-021-00515-3.

[47] C. Correia, R.O. Sousa, A.C. Vale, D. Peixoto, T.H. Silva, R.L. Reis, I. Pashkuleva, N.M. Alves, Adhesive and biodegradable membranes made of sustainable catechol-functionalized marine collagen and chitosan, Colloids Surf B Biointerfaces 213 (2022). https://doi.org/10.1016/j.colsurfb.2022.112409.

[48] C. Correia, D.S. Da Costa, A.R. Inácio, A.C. Vale, D. Peixoto, T.H. Silva, R.L. Reis, I. Pashkuleva, N.M. Alves, Adhesive and Antibacterial Films Based on Marine-Derived Fucoidan and Chitosan, ACS Sustain Chem Eng 10 (2022) 16770–16779. https://doi.org/10.1021/acssuschemeng.2c05144.

[49] S. Gimondi, R.L. Reis, H. Ferreira, N.M. Neves, Microfluidic-driven mixing of high molecular weight polymeric complexes for precise nanoparticle downsizing, Nanomedicine 43 (2022). https://doi.org/10.1016/j.nano.2022.102560.

[50] I. Serrano-Sevilla, Á. Artiga, S.G. Mitchell, L. De Matteis, J.M. de la Fuente, Natural polysaccharides for siRNA delivery: Nanocarriers based on chitosan, hyaluronic acid, and their derivatives, Molecules 24 (2019). https://doi.org/10.3390/molecules24142570.

[51] K.N. Clayton, J.W. Salameh, S.T. Wereley, T.L. Kinzer-Ursem, Physical characterization of nanoparticle size and surface modification using particle scattering diffusometry, Biomicrofluidics 10 (2016) 1–14. https://doi.org/10.1063/1.4962992.

[52] S. Boddohi, N. Moore, P.A. Johnson, M.J. Kipper, Polysaccharide-Based Polyelectrolyte Complex Nanoparticles from Chitosan , Heparin , and Hyaluronan, (2009) 1402–1409.

[53] Y. Agrawal, V. Patel, Nanosuspension: An approach to enhance solubility of drugs, J Adv Pharm Technol Res 2 (2011) 81. https://doi.org/10.4103/2231-4040.82950.

[54] H.T. Phan, A.J. Haes, What Does Nanoparticle Stability Mean? HHS Public Access, J Phys Chem C Nanomater Interfaces 123 (2019) 16495–16507. https://doi.org/10.1021/acs.jpcc.9b00913.What.

[55] S.L. Percival, S. McCarty, J.A. Hunt, E.J. Woods, The effects of pH on wound healing, biofilms, and antimicrobial efficacy, Wound Repair Regen 22 (2014) 174–186. https://doi.org/10.1111/wrr.12125.

[56] B. Nagoba, A. Gavkare, A. Rayate, S. Mumbre, A. Rao, B. Warad, N. Nanaware, N. Jamadar, Role of an acidic environment in the treatment of diabetic foot infections: A review, World J Diabetes 12 (2021) 1539–1549. https://doi.org/10.4239/wjd.v12.i9.1539.

[57] P. Sim, X.L. Strudwick, Y.M. Song, A.J. Cowin, S. Garg, Influence of Acidic pH on Wound Healing In Vivo: A Novel Perspective for Wound Treatment, Int J Mol Sci 23 (2022). https://doi.org/10.3390/ijms232113655.

[58] D.G. Metcalf, M. Haalboom, P.G. Bowler, C. Gamerith, E. Sigl, A. Heinzle, M.W.M. Burnet, Elevated wound fluid pH correlates with increased risk of wound infection, Wound Medicine 26 (2019). https://doi.org/10.1016/j.wndm.2019.100166.

[59] R. Strohal, M. Mittlbö, G. Hä, The Management of Critically Colonized and Locally Infected Leg Ulcers with an Acid-Oxidizing Solution: A Pilot Study, n.d.

[60] J. Tan, S. Shah, A. Thomas, H.D. Ou-Yang, Y. Liu, The influence of size, shape and vessel geometry on nanoparticle distribution, Microfluid Nanofluidics 14 (2013) 77–87. https://doi.org/10.1007/s10404-012-1024-5.

[61] J.W. Hickey, J.L. Santos, J.M. Williford, H.Q. Mao, Control of polymeric nanoparticle size to improve therapeutic delivery, Journal of Controlled Release 219 (2015) 536–547. https://doi.org/10.1016/j.jconrel.2015.10.006.

[62] D.M. Ibegbu, A. Boussahel, S. Cragg, J. Tsibouklis, E. Barbu, Nanoparticles of alkylglyceryl dextran and poly(ethyl cyanoacrylate) for applications in drug delivery: preparation and characterization, Journal of Polymeric Materials and Polymeric Biomaterials 66 (2017) 265–279. https://doi.org/https://doi.org/10.1080/00914037.2016.1201827.

[63] D.S. Nikam, S. V. Jadhav, V.M. Khot, R.S. Ningthoujam, C.K. Hong, S.S. Mali, S.H. Pawar, Colloidal stability of polyethylene glycol functionalized Co 0.5Zn0.5Fe2O4 nanoparticles: Effect of pH, sample and salt concentration for hyperthermia application, RSC Adv 4 (2014) 12662–12671. https://doi.org/10.1039/c3ra47319h.

[64] J.C. Dumville, B.A. Lipsky, C. Hoey, M. Cruciani, M. Fiscon, J. Xia, Topical antimicrobial agents for treating foot ulcers in people with diabetes, Cochrane Database of Systematic Reviews 2017 (2017). https://doi.org/10.1002/14651858.CD011038.pub2.

[65] S. Rittenhouse, S. Biswas, J. Broskey, L. McCloskey, T. Moore, S. Vasey, J. West, M. Zalacain, R. Zonis, D. Payne, Selection of retapamulin, a novel pleuromutilin for topical use, Antimicrob Agents Chemother 50 (2006) 3882–3885. https://doi.org/10.1128/AAC.00178-06.

[66] M. Stańkowska, K. Garbacz, A. Korzon-Burakowska, M. Bronk, M. Skotarczak, A. Szymańska-Dubowik, Microbiological, Clinical and Radiological Aspects of Diabetic Foot Ulcers Infected with Methicillin-Resistant and-Sensitive Staphylococcus aureus, Pathogens 11 (2022). https://doi.org/10.3390/pathogens11060701.

[67] H. Galkowska, A. Podbielska, W.L. Olszewski, E. Stelmach, M. Luczak, G. Rosinski, W. Karnafel, Epidemiology and prevalence of methicillin-resistant Staphylococcus aureus and Staphylococcus epidermidis in patients with diabetic foot ulcers: Focus on the differences between species isolated from individuals with ischemic vs. neuropathic foot ulcers, Diabetes Res Clin Pract 84 (2009) 187–193. https://doi.org/10.1016/j.diabres.2009.02.008.

[68] P. Dam, M. Celik, M. Ustun, S. Saha, C. Saha, E.A. Kacar, S. Kugu, E.N. Karagulle, S. Tasoglu, F. Buyukserin, R. Mondal, P. Roy, M.L.R. Macedo, O.L. Franco, M.H. Cardoso, S. Altuntas, A.K. Mandal, Wound healing strategies based on nanoparticles incorporated in hydrogel wound patches, RSC Adv 13 (2023) 21345–21364. https://doi.org/10.1039/d3ra03477a.

Declaration of interests

☒The authors declare that they have no known competing financial interests or personal relationships that could have appeared to influence the work reported in this paper.

☐The authors declare the following financial interests/personal relationships which may be considered as potential competing interests:

Highlights

- Hyaluronic acid was successfully methacrylated (HAMA) with a degree of modification of 20%.
- Nanoparticles were produced from HAMA and Chitosan by photo-crosslinking.
- The antimicrobial agent bacitracin was encapsulated in the nanoparticles with a high efficiency.
- Bacitracin-loaded nanoparticles demonstrated a pronounced antibacterial and antibiofilm effect.
- Bacitracin-loaded nanoparticles showed a positive effect on the proliferation of mammalian cells (L929).
- The developed nanoparticles are a promising alternative therapeutic in treating chronic wounds.